Fuzzy Predictive DTC of Induction Machines With Reduced Torque Ripple and High-Performance Operation

Alberto Berzoy, *Student Member, IEEE*, Johnny Rengifo, and Osama Mohammed, *Fellow, IEEE*

***Abstract*—This paper proposes an enhanced strategy for direct torque control (DTC) combining artificial intelligent (AI) and predictive algorithms. The advantages of this merge are in the solution of closed-loop controlled induction machine (IM) problems. Predictive DTC (P-DTC) methods reduce the high torque ripple and improve the performance at both starting condition and low mechanical speed operation. However, P-DTC depends on the IM parameter's knowledge. The approach here is the introduction of fuzzy logic control with dynamic rules based on the P-DTC law's to reduce the parameter dependency and improve the performance of P-DPC. Additional comparative performance study of eight modulation strategies under the proposed fuzzy-predictive DTC (FP-DTC) is conducted. It results that the space-vector modulation (SVM) is the most suitable scheme with the best combination of criteria such stator current total harmonic distortion, switching losses and dynamic behavior. The parameter dependency of the FP-DTC is tested by a sensitivity analysis which corroborates the robustness of the proposed control. For verification purposes, simulations of the DTC, P-DTC, and FP-DTC were conducted and compared. Experimental results for the three controllers and two modulations (pulse width modulation and SVM) confirm the expected performance of the proposed control algorithm and modulation assessment study.**

***Index Terms*—Direct torque control, fuzzy logic, induction machines, modulation strategies, predictive control.**

I. Introduction

INDUCTION machines (IMs) are relevant in industrial applications and they are ideal for harsh environments due to its robustness, ruggedness, high efficiency, lower cost, and maintenance. In the history of IM, the first controllers dictate to connect the IM directly to the mains or to scalar controllers such as the voltage-frequency driver. The last one suffers from limitations at low speed and poor torque response [1]. The emergence of vector control techniques (VCTs) moderately solves the IM control problems. One of the most famous VCTs is the field-oriented control (FOC) presented in [2]. This strategy grants control of the rotor flux and torque independently, acting over the stator current phase and quadrature components. Typically, the FOC design is simple but its performance depends on the knowledge of the IM parameters and the load variations. Moreover, rotor flux observers are difficult to design when the IM's parameters vary with the frequency and temperature. Solutions for these problems were proposed in [3] and [4].

More recent VCTs are the direct self-control (DSC) and direct torque control (DTC) proposed in [5] and [6], respectively. The DSC is better suited for high power and low switching frequency applications. The DTC is widely utilized and best suited for low and medium power and high switching frequency applications. DTC produces rapid torque response whereas keeping the IM stator flux and torque decoupled. The main disadvantages of DTC are the large torque ripple, its high start-up current, variable switching frequency, and poor performance under overload and low-speed operation. Plenty of research has been conducted to improve the DTC performance. DTC alterations are presented in [7] and [8] for enhancing the starting condition and the low-speed operation. Solutions to these drawbacks are proposed in [9]–[12] with predictive strategies but they are parameter dependent. In [13], a DTC modification is presented to reduce the torque ripple and enhance the response of the control under overload condition with the price of higher parameter sensitivity. A modulated hysteresis DTC is proposed in [14] to achieve constant switching frequency and decrease the torque oscillations. In [15]–[16], fuzzy controllers are proposed to reduce torque ripple and limit the stator current.

In this paper, a torque controller that integrates the advantages of fuzzy logic controller (FLC) and model predictive control (MPC) is proposed. The FLC helps in the reduction of the torque ripple with significant decrement of the parameters dependency and limitation of the inrush current. The MPC technique aims in the improvement of the performance at both starting condition and low-speed operation. In this approach, the FLC rules are based on a predictive DTC (P-DTC) where the main idea is to observe the nonperpendicular quadrants formed by the two lines of constant torque and constant stator flux magnitude drawn in the complex vector plane (CVP) of the voltage source inverter (VSI). A comparative study is performed among the classical DTC, P-DTC, and the proposed fuzzy-predictive DTC (FP-DTC) showing the advantages and disadvantages of every

Manuscript received September 29, 2016; revised February 15, 2017; accepted March 20, 2017. Date of publication April 3, 2017; date of current version December 1, 2017. This work was supported in part by grants for the Office of Naval Research and in part by the U.S. Department of Energy. Recommended for publication by Associate Editor K.-B. Lee. *(Corresponding Author: Alberto Berzoy.)*

A. Berzoy and O. Mohammed are with the Energy Systems Research Lab., ECE Department, Florida International University, Miami, FL 33199 USA (e-mail: aberz001@fiu.edu; mohammed@fiu.edu).

J. Rengifo is with the Simon Bolivar University, Energy Conversion and Delivery Department, Caracas 1080, Venezuela (e-mail: jwrengifo@usb.ve).

Color versions of one or more of the figures in this paper are available online at http://ieeexplore.ieee.org.

Digital Object Identifier 10.1109/TPEL.2017.2690405

control under diverse torque profiles and different load conditions. An assessment analysis over eight different continues and discontinues modulation strategies is performed. A parameter sensibility examination is conducted to corroborate the thesis of FP-DTC is robust to the parameter variations. Finally, experimental results are conducted confirming all the expected performance and hypothesis.

II. Predictive Direct Torque Control

The P-DTC's objective is to control the electromagnetic torque and the magnitude of the stator flux-linkage space-vector (SV) independently. Thus, it is convenient to represent the IM dynamic state-space equations in terms of the stator current SV $\mathbf{i_s}$ and stator flux-linkage SV $\boldsymbol{\lambda}_\mathbf{s}$, as follows:

$$\begin{aligned} p\mathbf{i_s} &= \frac{\mathbf{v_s}}{\hat{L}_s} - \left(\frac{L_s}{L_r}\frac{R_r}{\hat{L}_s} + \frac{R_s}{\hat{L}_s} - jP\omega_m\right)\mathbf{i_s} + \left(\frac{R_r}{L_r} - jP\omega_m\right)\frac{\boldsymbol{\lambda}_\mathbf{s}}{\hat{L}_s} \\ p\boldsymbol{\lambda}_\mathbf{s} &= \mathbf{v_s} - R_s\mathbf{i_s} \\ p\omega_m &= \frac{1}{J}\left(T_e - T_m\right) \end{aligned} \tag{1}$$

where R_r and R_s are the resistances, and L_r and L_s are the self-inductances of the rotor and stator, respectively; $\hat{L}_s = L_s - \frac{L_{sr}^2}{L_r}$, L_{sr} is the mutual inductance, ω_m is the mechanical speed, $T_e = P\boldsymbol{\lambda}_\mathbf{s} \times \mathbf{i_s}$ and T_m are the electrical and mechanical load torque respectively; P is the number pole pairs, J is the inertia of the machine and the stator SV $\mathbf{i_s}$, $\mathbf{v_s}$ and $\boldsymbol{\lambda}_\mathbf{s}$ are written in complex-vector notation referred to stationary $(\alpha\beta)$ reference frame, thusly $\mathbf{f_s} = f_{\alpha s} + jf_{\beta s}$; $\mathbf{f_s} = \{\mathbf{i_s}, \mathbf{v_s}, \boldsymbol{\lambda}_\mathbf{s}\}$; and p is the time-derivative operator. The transformation from the primitive coordinates (*abc*) to the stationary $(\alpha\beta)$ reference frame is Hermitian or power conservative.

For the particular case of the IM and on the basis of MPC theory [17], it is possible to foresee the output error, $\boldsymbol{y} = [T_e, |\boldsymbol{\lambda}_\mathbf{s}|]$, in the next cycle of control (t_{k+1}), as the output have a relative degree $\{1,1\}$ which is defined everywhere except at $|\boldsymbol{\lambda}_\mathbf{r}| = 0$ [18]. This anticipation can be computed based on the time derivatives of the two outputs as follows:

$$\begin{aligned} pT_e &= p\left(P\boldsymbol{\lambda}_\mathbf{s} \times \mathbf{i_s}\right) \\ p\left|\boldsymbol{\lambda}_\mathbf{s}\right| &= \frac{2}{|\boldsymbol{\lambda}_\mathbf{s}|}\boldsymbol{\lambda}_\mathbf{s} \times j\left(\mathbf{v_s} - R_s\mathbf{i_s}\right) \end{aligned} \tag{2}$$

$$\begin{aligned} pT_e = &\left[\frac{\left(\mathbf{v_s} - jNP\ \omega_m\boldsymbol{\lambda}_\mathbf{s}\right)}{1/P} \times \left(\mathbf{i_s} - \frac{\boldsymbol{\lambda}_\mathbf{s}}{\hat{L}_s}\right)\right. \\ &\left. - \left(\frac{L_sR_r + L_rR_s}{L_r\hat{L}_s}\right)T_e\right] \\ p\left|\boldsymbol{\lambda}_\mathbf{s}\right| = &\frac{2}{|\boldsymbol{\lambda}_\mathbf{s}|}\boldsymbol{\lambda}_\mathbf{s} \times j\left(\mathbf{v_s} - R_s\mathbf{i_s}\right) \end{aligned} \tag{3}$$

where $\mathbf{a} \times \mathbf{b} = a_\alpha b_\beta - b_\alpha a_\beta$ is the cross-product operation between two vectors.

The selection of the best VSI vector (*input space* $\mathbf{u} = \mathbf{v_s}$) is achieved by the comparison of the values resulting from the cost function (ψ) defined in (4), for the seven inverter switching states or input control action (ICA)

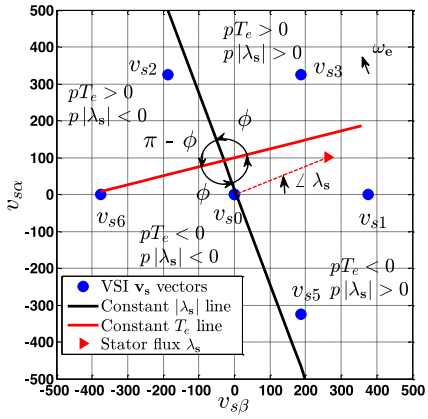

Fig. 1. Torque and stator flux constants variation lines at the CVP.

$$\psi^i = k_1\left(\{pT_eT_s\}^i - \Delta T_e\right)^2 + k_2\left(\{p\left|\boldsymbol{\lambda}_\mathbf{s}\right|T_s\}^i - \Delta\left|\boldsymbol{\lambda}_\mathbf{s}\right|\right)^2 \tag{4}$$

where $(\Delta T_e,\ \Delta|\boldsymbol{\lambda}_\mathbf{s}|)$ are the actual output errors, $(\{pT_eT_s\}^i,$ $\{p|\boldsymbol{\lambda}_\mathbf{s}|T_s\}^i)$ are the predicted errors or variable incremental, the superscript $i = \{1,\ \ldots, 7\}$ indicates the VSI states or ICA $v_{si} = \{v_{s1},\ \ldots, v_{s7}\}$ as shown in Fig. 1 (blue dots), k_1 and k_2 are weighting constants. The index of the minimum cost function value $[\psi^1, \ldots, \psi^7]$ determines the index of the ICA at the next instant t_{k+1}.

Setting both time derivatives in (3) equal to zero ($pT_e = 0$ and $p|\boldsymbol{\lambda}_\mathbf{s}| = 0$), two linear voltage equations can be expressed as function of the inverter voltages or *input space* $(v_{s\alpha}, v_{s\beta})$ as in (5). Plotting these equations in the CVP for one cycle of control, they would be as shown in Fig. 1

$$\begin{aligned} v_{s\beta_\lambda} &= R_si_{s\beta} - \frac{\lambda_{s\alpha}}{\lambda_{s\beta}}\left(v_{s\alpha_\lambda} - R_si_{s\alpha}\right) \\ v_{s\beta_T} &= \frac{\left(\hat{L}_si_{s\beta} - \lambda_{s\beta}\right)}{\left(\hat{L}_si_{s\alpha} - \lambda_{s\alpha}\right)}\left(v_{s\alpha_T} - \frac{\hat{L}_sA}{\hat{L}_si_{s\beta} - \lambda_{s\beta}}\right) \end{aligned} \tag{5}$$

where $A = \frac{\left(\frac{L_s}{L_r}R_r + R_s\right)T_e}{P\hat{L}_s} - P\omega_m\left(\boldsymbol{\lambda}_\mathbf{s} \times j\mathbf{i_s}\right) + \frac{P\omega_m\left|\boldsymbol{\lambda}_\mathbf{s}\right|^2}{\hat{L}_s}$.

These two linear equations represent the constant torque variation $(v_{s\beta_T})$ and constant magnitude of the stator flux vector variation $(v_{s\beta_\lambda})$. The constant variation is due to their deduction originates from the time derivative cancellation. Each plotted equation in the CVP divide the *input space* in two subspaces where a perpendicular ICA to these lines will create the maximum change possible in the output variable. When the inverter ICA is over (under) one of the lines then the trend is to increment (decrement) this variable. Generally, these two lines are not perpendicular between each other and they normally do not intersect in the CVP origin, hence four irregular quadrants (four sub-spaces) are created in every cycle of control (t_k). This irregularity generates an imbalanced number of input voltage vectors for each of the subspaces created. In classical DTC, it is assumed that these lines are perpendicular and in this way even number of input voltage vectors is obtained in each cycle of control and in each

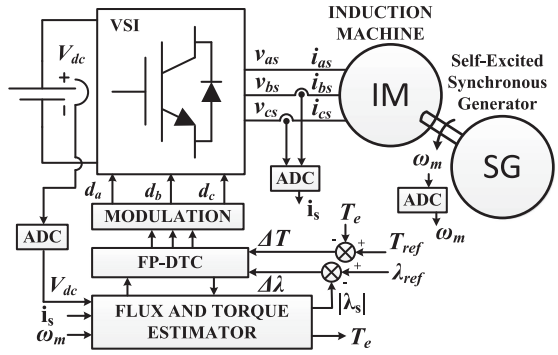

Fig. 2. Block diagram of the complete system.

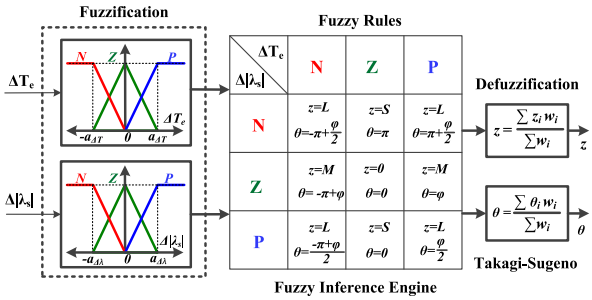

Fig. 3. Block diagram of the proposed FP-DTC.

quadrant [18]. The four cases of increasing or decreasing the output errors $\Delta T_e = T_{ref} - T_e$ and $\Delta|\boldsymbol{\lambda}_\mathbf{s}| = \lambda_{ref} - |\boldsymbol{\lambda}_\mathbf{s}|$ are as follows: $\Delta T_e > 0$ and $\Delta|\boldsymbol{\lambda}_\mathbf{s}| > 0, \Delta T_e > 0$ and $\Delta|\boldsymbol{\lambda}_\mathbf{s}| < 0, \Delta T_e < 0$ and $\Delta|\boldsymbol{\lambda}_\mathbf{s}| > 0, \Delta T_e < 0$ and $\Delta|\boldsymbol{\lambda}_\mathbf{s}| < 0$. The angle in between these two lines is defined as ϕ (see Fig. 1).

III. Fuzzy-Predictive Direct Torque Control

An efficient solution for mitigating the issues of the classical DTC algorithm is to apply FLC as in [15]. The FL-based DTC provides an adaptive variation of the duty cycle based on the switching table proposed by Noguchi [6], however, the rules are fixed making it to drag some drawbacks of classical DTC such as poor performance at both starting and low-speed operation.

In the proposed FP-DTC, the contribution is the integration of FLC with an MPC strategy which allows not only adaptive variation but also dynamic rules. The main limitation of FLC is the requirement of high-speed microprocessor ability with large memory size and the lack of the design strategies, most of FL system parameters are determined intuitively based on the designer and/or the operator experience. To solve the first problem, the FLC system is designed by choosing minimum number of linear membership functions (MFs) for each input and using Takagi–Sugeno (T–S) fuzzy inference system (FIS) technique for calculating the control decision. The second problem is inherently solved as the designed fuzzy rules are dynamic and depend on the defined angle ϕ. A block diagram for the complete system is depicted in Fig. 2. In Fig. 3, a detailed block diagram of the FIS is shown. The FIS is a zero-order T–S with two inputs (ΔT_e and $\Delta|\boldsymbol{\lambda}_\mathbf{s}|$) and one output ($\mathbf{v_{Fuzzy}} = ze^{j\theta}$). The universe of discourse of each input is described by three

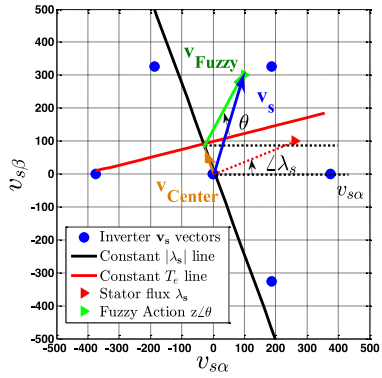

Fig. 4. Vector summation of fuzzy output and correction.

MF (N, Z, and P). The fuzzy rules, that define the relationship between the fuzzy inputs and output, are chosen as a function of the angle ϕ. The matrix rule is the one presented in Fig. 3. Each fuzzy rule has two parameters for the two outputs: magnitude (z) and angle (θ); e.g., assume $\Delta T_e > 0$ and $\Delta|\boldsymbol{\lambda}_\mathbf{s}| > 0$, thus $\text{MF}_T = P$ and $\text{MF}_\lambda = P$. The matrix rules indicate $z = L$ and $\theta = \phi/2$. If the two lines of constant torque and flux are orthogonal and centered at the CVP, the rule would be $\theta = \pi/2$ and the control will be the same as the one proposed in [15]. In this FLC, the rules are dynamic and varying at every period of control as a function of the angle ϕ, which changes with the IM position and operative conditions. The angle ϕ is calculated from (5).

The FLC output need to be conditioned for the modulation technique, thus and so two conditioning methods can be implemented. Using (6) for mounting the fuzzy output over the flux-linkage SV or (7) that is a vector summation as shown in Fig. 4

$$\begin{aligned} v_{s\alpha} &= z\cos\left(\theta + \angle\boldsymbol{\lambda}_\mathbf{s}\right) \\ v_{s\beta} &= z\sin\left(\theta + \angle\boldsymbol{\lambda}_\mathbf{s}\right) \end{aligned} \tag{6}$$

$$\mathbf{v_s} = \mathbf{v_{Center}} + \mathbf{v_{Fuzzy}} \tag{7}$$

where $\mathbf{v_{Center}}$ is the vector from the center of the CVP to the point where the lines of constant torque and constant magnitude of flux crosses. This vector can be realized by making equal the two voltage equations of (5), in such a way $v_{s\beta_\lambda} = v_{s\beta_T}$. Therefore the coordinates of this cross-point are as follows:

$$\begin{aligned} v_{Center\beta} &= \frac{R_s\left(i_\beta - \frac{\lambda_{s\beta}}{\hat{L}_s}\right)\boldsymbol{\lambda}_\mathbf{s} \times j\mathbf{i_s} - A\lambda_{s\beta}}{\boldsymbol{\lambda}_\mathbf{s} \times j\mathbf{i_s} - P\omega_m\frac{|\boldsymbol{\lambda}_\mathbf{s}|^2}{\hat{L}_s}} \\ v_{Center\alpha} &= R_s i_{s\alpha} - \frac{\lambda_{s\beta}}{\lambda_{s\alpha}}\left(v_{Center\beta} - R_s i_{s\beta}\right). \end{aligned} \tag{8}$$

The computation, in the first case, is two trigonometric functions and, in the last case, is just the calculation of two linear equations and their tangents (lines slope's). The advantage of this proposed controller is that it corrects the control angle of the ICA compared with the classic table of DTC which sometimes is erratic causing the well-known big torque ripple and poor

performance. Also, FLC decrease the parameter dependency of the predictive control.

IV. Performance Assessment of Different Pulse Width Modulation (PWM) Strategies

The goal of any modulation scheme is to achieve the desired voltage reference in the CVP with additional reduction of stator current ripple, switching losses, common-mode voltages, electromagnetic interference, etc. In this sense, much research has been devoted toward the development of efficient ways of controlling the VSI with additional low computational burden in its implementation [19]. In general, the modulation strategies can be categorized in continuous and discontinuous PWM due to the different choices for the zero vector duty cycle subdivision [19], [20]. Despite the fact that there is an infinite number of possibilities to subdivide the zero vector duty cycle (δ_z), the performance and constraints of practical PWM in VSI drives reduce this to a finite number of viable choices [20]. The continuous modulations are sinusoidal PWM (SPWM) and SV modulation (SVM) and the discontinuous are DPWM0, DPWM1, DPWM2, DPWM3, DPWMax, and DPWMin, which have different clamp regions that align the reference voltage peak. DPWM1 is suitable for unity power factor, DPWM0 and DPWM2 are efficient for 30° leading and lagging power factors, respectively, and DPWM3 is a distortion-optimized modulation [21]. Deep analysis of these modulation strategies is found in [20] and their generalization is described in [19].

In this paper, the behavior of all these modulation schemes using the generalized algorithm presented in [19] is studied. The generalized algorithm is programmed and simulated. A modulator is characterized by different performance parameters [21], i.e., generated current harmonics, maximum modulation index, switching frequency, switching losses, and dynamic response. The performance criteria for the assessment, in this paper, consider three parameters: switching losses, current distortion, and dynamic response.

A. Switching Losses

The switching losses evaluation is performed in the same way as [21] assuming that the VSI has switching losses that vary linearly with the amplitude of the current. Thus, the average value of the switching power losses ($P_{\rm sw}$) over a fundamental period is assessed below

$$P_{\rm sw} = \frac{1}{2\pi}\frac{1}{2}\left(V_{\rm dc}.\left(t_{\rm on}+t_{\rm off}\right).f_s.\int_0^{2\pi}\left|I_F\left(\theta\right)\right|d\theta\right) \quad (9)$$

where $V_{\rm dc}$ is the dc-link voltage, $t_{\rm on}$ and $t_{\rm off}$ are the respective turn-on and off intervals of the switching devices that can be found in its datasheet, f_s is the switching frequency, I_F is the output inverter current, and $|\cdot|$ is the absolute value function.

B. Current Distortion and Dynamic Response

The current distortion is conducted by the computation of the total harmonic distortion (THD) of the stator current of the IM. For the dynamic behavior, the mean absolute error (MAE) and root mean square error (RMSE) for the electromagnetic torque and magnitude of the stator flux-linkage SV is computed. For these variables, the MAE and RMSE are calculated for the torque between the instantaneous torque reference ($T_{e\_ref\_k}$) and the instantaneous electric torque T_{e_k} and for the flux-linkage between the flux-linkage reference ($\lambda_{s\_ref\_k}$) and magnitude of the flux-linkage ($|\boldsymbol{\lambda}_{\mathbf{s\_k}}|$). As follows, the instantaneous errors are computed as (10) and MAE and RMSE as

$$e_{k\_T} = \frac{T_{e\_ref\_k} - T_{e\_k}}{\text{Rated Torque}} \qquad e_{k\_\lambda} = \frac{\lambda_{s\_ref\_k} - |\boldsymbol{\lambda}_{\mathbf{s\_k}}|}{\lambda_{s\_ref\_k}} \quad (10)$$

$$\text{MAE} = \frac{1}{N}\sum\nolimits_{k=1}^{N}|e_{k\_x}| \qquad \text{RMSE} = \sqrt[2]{\frac{1}{N}\sum_{k=1}^{N}e_{k\_x}^2} \quad (11)$$

where $x = \{T, \lambda\}$.

TABLE I
IM Parameters and Nameplate Rating

Param.	Value	Param.	Value	Rating	Value	Rating	Value
L_{ls}	3.08 mH	R_s	1.506 Ω	P	1.5 kW	PF	0.83
L_{lr}	3.46 mH	R_r	0.6172 Ω	V	208 V	Poles Pairs	2
L_m	119.22 mH	J_m	0.13 kgm^2	I	5.9 A	n_r	1750 r/min

V. Simulation and Experimental Results

In order to compare the performance of the proposed FP-DTC, a simulation and experimental test comparison among classical DTC, P-DTC, and proposed FP-DTC is carried out. The IM parameters used in this study are found by characterizing the induction motor at the starting condition under a step of ac voltage, the procedure followed for the parameter estimation is proposed in [22] and [23]. The parameter estimation method adjusts the instantaneous input impedance motor during a start-up. For all the simulations and experimental tests, the machine is belt coupled with a self-excited synchronous generator for emulating the loading conditions. The parameter estimation was performed for the no load and loaded case to calculate the inertia of the load. Finally, the model parameters are presented in Table I and these values are used in the simulations. The simulations are conducted in Simulink/MATLAB environment.

The simulation and experimental implementation were conducted under the same conditions of dc-link capacitor voltage $V_{\rm dc} = 300$ V, switching frequency $f_s = 10$ kHz, and current limitation $I_{\rm limit} = 30/\sqrt{2}$ A$_{\rm rms}$. For purposes of accuracy and fairness comparison of the simulation and experimental results, the simulation step time was 10 μs but the control algorithm operates at 0.1 ms. The PWM in both simulation and experimental is at 10 kHz and centered aligned.

For purposes of control performance verification, a torque profile similar to the one found in electric vehicles applications is implemented. Simulation and experimental tests are conducted for the three controllers. The torque profile starts with a step at 8 N · m which is the rated torque from the name plate of the machine, then after 2 s, a down step of torque reach the 4 N · m.

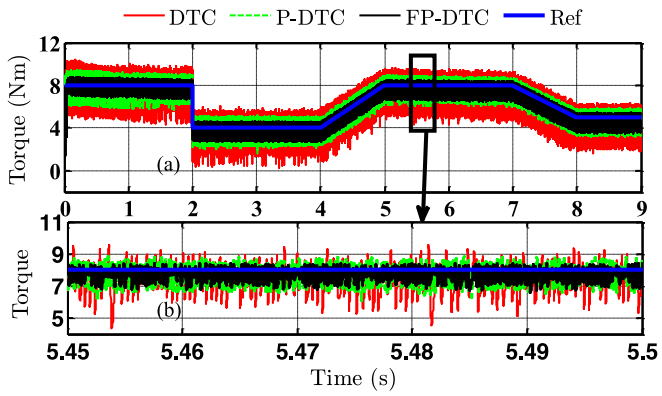

Fig. 5. (a) Simulation results for comparison of the electromagnetic torque among DTC, P-DTC, and FP-DTC. (b) Zoom of (a).

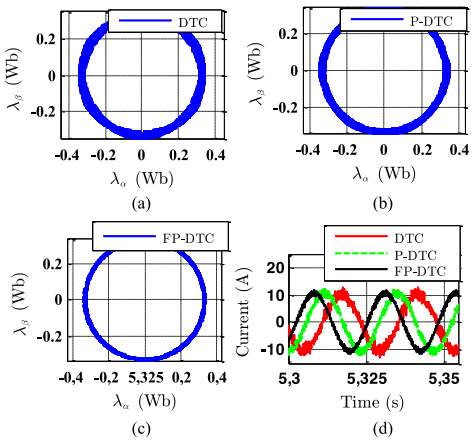

Fig. 6. Simulation results of the stator flux locus (a) DTC, (b) PDTC, (c) FPDTC, and (d) stator current comparison among the strategies.

A ramp increases the profile 2 s later until the nominal torque again keeping it for 2 more s and a down ramp ends the profile in 5 N · m (see Fig. 5(a) for simulation and 8(a) for experimental). The flux reference in all the simulations and experiments is $\lambda_{s\_ref} = 0.33$ Wb.

A. Simulation Results

In Fig. 5(a), the torque reference and the electromagnetic torque produced by the IM controlled by DTC, P-DTC, and FP-DTC is presented. In this figure, it can be noticed that the dynamics of the three algorithms are very fast; however, the ripple is not the same for the three techniques. In Fig. 5(b), a zoom of the electromagnetic torque for the three strategies is shown and it is clear that the classical DTC suffer for two problems: steady-state error and high torque ripple. In the other hand, the P-DTC corrects the steady-state error and reduces the torque ripple, nonetheless, the FP-DTC is even better. The high torque ripple in DTC is produced by the selection of the nonoptimum voltage vector while FP-DTC chooses the control vector using the constant torque and flux lines on the CVP allowing to reduce the torque ripple. The locus of the stator flux vector for the DTC, P-DTC, and FP-DTC is depicted in Fig. 6(a)–(c). The three loci present coincident response, although, the locus of FP-DTC has less ripple. In Fig. 6(d), a zoom for the phase *a* current for the three controllers is shown in steady-state regime. It can be observed that the currents are sinusoidal and the current ripple of DTC is higher than P-DTC and FP-DTC, as well as the current ripple of P-DTC is higher than FP-DTC.

A comparison of the different control methods (DTC, P-DTC, and FP-DTC) in respect to THD and power losses is presented in Table II. For the THD analysis, a preliminary FFT, the stator current is performed to calculate the fundamental component in permanent regime. This fundamental frequency result the same for the three controllers at 42 Hz. For the THD, two cycles of the signal are studied at 4.5 s.

TABLE II
MAXIMUM CRITERIA VALUES FOR EACH CONTROL TECHNIQUE

Control	MAE T_e (%)	RMSE T_e (%)	MAE $\lvert\boldsymbol{\lambda}_s\rvert$ (%)	RMSE $\lvert\boldsymbol{\lambda}_s\rvert$ (%)	P_{loss} (W)	THD I_s (%)
FPDTC	3.23	6.31	0.75	2	0.0505	8.84
PDTC	6.07	7.77	1.28	1.91	0.0442	18.81
DTC	10.2	13.3	2	3.17	0.0457	25.76

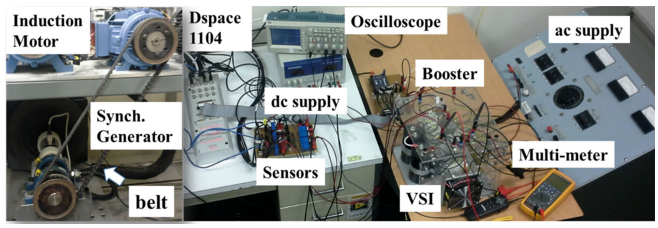

Fig. 7. Experimental setup.

B. Experimental Results

In order to compare the performance of the proposed FP-DTC, an experimental comparison was accomplished. Fig. 7 presents the experimental test rig which is composed by a computer, dSpace 1104, dc power supply for the control, booster for increasing the pulses (0 V off 5 V on) from the dSpace to the IGBT drivers (–10 V off 15 V on), sensor board (LEM voltage and current transducers), oscilloscope Tecktronics, ac autotransformer, motor-generator set (motor WEG W21, generator Yanan SLG-164B) and a VSI which consist of Semikron IGBTs (1200 V – 50 A), drivers, and two electrolytic capacitors of in series of 1200 μF and 525 V.

The experimental results for the torque profile response can be observed in Fig. 8(a). Fig. 8(b) presents a zoom of the response for a period of 50 ms. The experimental results are highly correlated with the simulation presented in Fig. 5(a) and (b). As it is expected, all the controllers have fast dynamic response, despite, DTC and P-DTC have more torque ripple and steady-state error than FP-DTC.

In Fig. 9, the loci of the stator flux SV for the DTC, P-DTC, and FP-DTC are presented. It can be seen, that the three loci present similar performance as expected from the simulation, however, FP-DTC demonstrates less ripple. In Fig. 9(d), the dc-link voltage is presented as it is not an ideal source like in

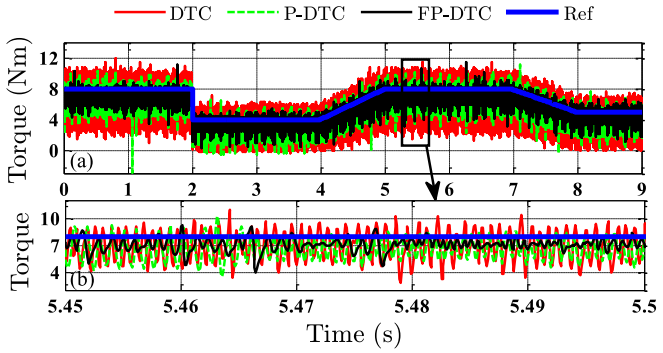

Fig. 8. (a) Experimental comparison of the electromagnetic torque among DTC, P-DTC, and FP-DTC. (b) Zoom of (a).

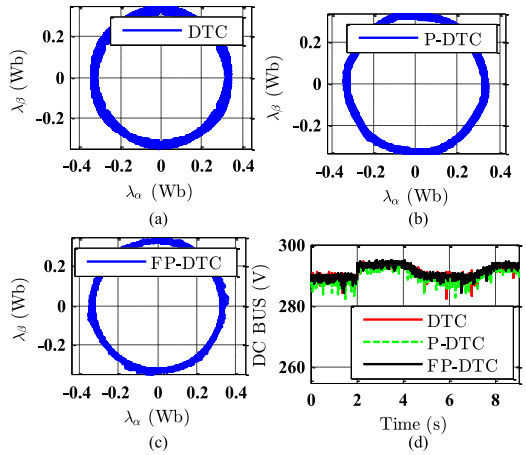

Fig. 9. Experimental comparison of the stator flux locus: (a) DTC. (b) PDTC. (c) FPDTC. (d) Stator current comparison among the strategies.

TABLE III
SIMULATION AND EXPERIMENTAL COMPARISON AMONG TORQUE, FLUX, AND CURRENT RIPPLES OF DTC, P-DTC AND FPDTC

	Simulation Results			Experimental Results		
	DTC	PDTC	FPDTC	DTC	PDTC	FPDTC
Torque Ripple (N·m)	4.5	2	1	6	2.5	1
Flux Ripple (Wb)	0.05	0.035	0.02	0.05	0.05	0.04
Current Ripple (A)	2	1.5	1	4	2	1

the simulation. The effect on these variations affects the torque response of the experimental resulting in higher torque ripple than simulations.

For final comparison among the three controllers and its correlation with the simulation results, a comparative result of the torque ripple, stator flux ripple, and current ripple is presented in Table III.

C. Sensitivity Analysis

The proposed control strategy adjusts the fuzzy rules base on the machine model, thereby to compute the FP-DTC algorithm the machine's parameters are required. A sensitivity analysis is presented to evaluate the robustness of the proposed controller under uncertainty in the IM parameters. The rotor resistance, leakages, and mutual inductances were change over a range of

TABLE IV
MAXIMUM MAE AND RMSE OF R_r, L_{ls}, L_{lr} AND L_m FOR 50% VARIATION ON THEIR VALUE

Param	Final Values $\Delta = +50\%$	MAE		Final Values $\Delta = -50\%$	MAE	
		T_e (%)	$\lvert\boldsymbol{\lambda}_s\rvert$ (%)		T_e (%)	$\lvert\boldsymbol{\lambda}_s\rvert$ (%)
L_{ls}	4.62 mH	5.16	0.74	1.54 mH	5.16	0.74
L_{lr}	5.29 mH	5.05	0.75	1.73 mH	503	0.67
L_m	178.83 mH	5.03	0.67	59.61 mH	5.03	0.67
R_r	0.9258 Ω	5.25	0.78	0.3086 Ω	5.04	0.70

TABLE V
MAXIMUM CRITERIA VALUES FOR EACH MODULATION TECHNIQUE

Modulation	MAE	RMSE	MAE	RMSE	THD	P_{loss}
	T_e (%)		$\lvert\boldsymbol{\lambda}_s\rvert$ (%)		I_s (%)	(W)
PWM	3.23	6.31	0.75	2.00	8.86	0.0505
SVM	2.39	5.81	0.71	1.98	5.67	0.0509
DPWM0	3.69	6.69	0.71	1.87	6.78	0.0510
DPWM1	7.05	11.45	0.77	2.23	10.30	0.0531
DPWM2	3.80	6.83	0.72	2.15	7.25	0.0506
DPWM3	3.41	6.42	0.70	1.89	7.30	0.0502
DPWMax	3.04	6.36	0.73	2.02	5.72	0.0516
DPWMin	2.79	6.04	0.71	1.94	5.56	0.0512

±50%. Each case was simulated using the same torque profile as in Section V-A. The MAE among the instantaneous torque reference and the instantaneous electric torque and magnitude of the stator flux reference and actual flux are presented in Table IV. The RMSE is omitted for simplification purposes.

As it can be noted from Table IV, the MAE is smaller than 6% indicating that the FPDTC is robust to the variation of the main parameters of the model. Also, it can be observed that the MAE for the flux is basically constant. Typically, the magnitude of the flux is a more stable variable than that of the electromagnetic torque.

D. PWM Strategies: Comparative Study

In this section, eight PWMs (SPWM, SVM, DPWM0, DPWM1, DPWM2, DPWM3, DPWMax, and DPWMin) were studied, simulated, and compared, as it is shown in Table V. For this comparison assessment, three criteria are considered: switching losses (P_{loss}), current distortion (THD I_s), and dynamic response (MAE and RMSE of T_e and $\lvert\boldsymbol{\lambda}_s\rvert$).

From Table V, it can be observed that the SVM presents the best dynamic performance in terms of less torque error and the second best stator flux error. In respect to the current distortion, DPWMin has the lowest THD, nevertheless, SVM has the following lowest value. For the power switching losses, the criteria give similar values of all the modulation techniques. DPWM3 presents the lower losses, per contra, SVM is not far from there. SVM is the fourth best technique. Therefore, in the combination of all the criteria, SVM is the one that presents the better behavior. In this fashion, SVM is chosen among the modulations for the real experimental comparison with the previous results.

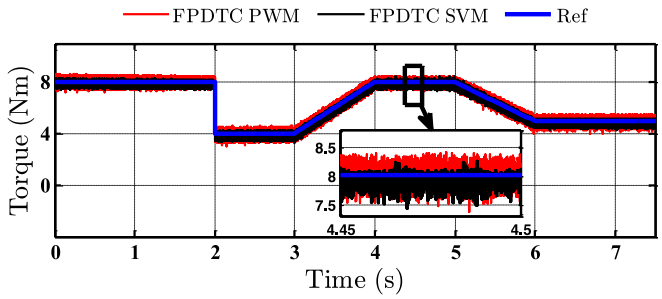

Fig. 10. Simulation comparison of the electromagnetic torque of FP-DTC between two modulation techniques: PWM and SVM.

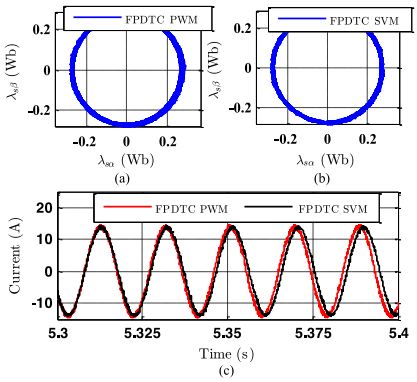

Fig. 11. Simulation comparison of FP-DTC between two modulation techniques. (a) Stator flux magnitude PWM. (b) Stator flux magnitude PWM. (c) Phase a current.

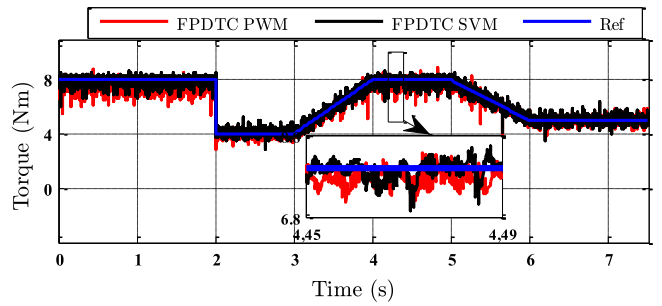

Fig. 12. Experimental comparison of the electromagnetic torque of FP-DTC between two modulation techniques: PWM and SVM.

E. Simulation and Experimental Results for the Comparative Assessment Between SVM and PWM

In this section, the experimental and simulation comparison results are presented between the selected modulation technique (SVM) and the original modulation used (PWM). The variables for the comparison are the same as used before: electromagnetic torque (see Figs. 10 and 12, simulation and experimental results, respectively), locus of the stator flux linkage (see Fig. 11(a), (b) for simulation, Fig. 13(a) and (b) for experimental results), stator phase *a* current (see Figs. 11(c) and 13(c), simulation and experimental results, respectively), and finally dc-link voltage (see Fig. 13(d) only experimental results).

Figs. 10 and 12 introduced a similar profile as the one presented in Figs. 5 and 8. From these figures, not only the good torque dynamic of the FP-DTC, but also the small torque ripple for both modulation techniques can be observed. In the zoom of these figures for simulation and experiments results, it can be seen that the SVM presents less torque ripple than the PWM method.

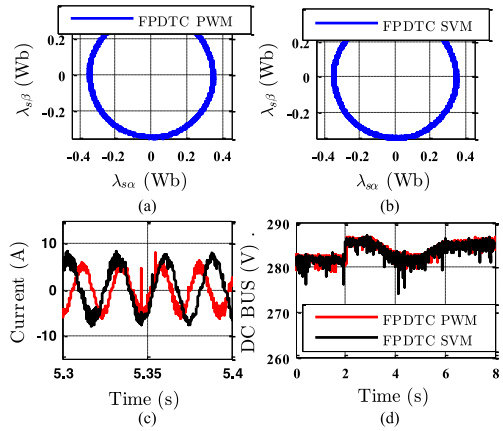

Fig. 13. Experimental comparison of FP-DTC between two modulation techniques. (a) Stator flux magnitude PWM. (b) Stator flux magnitude PWM. (c) Phase a current. (d) Dc-link voltage.

TABLE VI
MAXIMUM CRITERIA VALUES FOR EACH MODULATION TECHNIQUE

Modulations	MAE	RMSE	MAE	RMSE	THD
	T_e (%)		$\lvert\boldsymbol{\lambda}_s\rvert$ (%)		I_s (%)
PWM	25.09	31.34	1.89	2.31	5.59
SVM	19.62	25.40	1.94	2.10	4.98

The comparison of the locus for both simulation and experimental results, it is difficult to observe any difference between the SVM and PWM techniques, however, Table VI indicate better MAE and RMSE for the SVM modulation. From the simulation, the stator phase *a* currents are perfectly sinusoidal waveforms for the two modulation strategies. From the experimental results, some noise harmonic which is similar for both techniques can be noted. Also, Table VI indicates the numerical values that corroborate the results. Finally, the dc-link voltage is compared for the experimental results in Fig. 13(d) where congruent behavior is found for the two modulations techniques.

VI. CONCLUSION

An innovative and simple control strategy based on the integration of an FLC algorithm with minimum and linear MF with a predictive methodology is presented. The advantages of both techniques are exploited to improve the drawbacks and performance of the direct torque controller. Simulations and experimental results show an improvement in the control performance of the torque including ripple and steady-state error reduction and a satisfactory performance at the low-speed region. The proposed control was tested under $\pm 50\%$ variation of the IM parameters obtaining similar results and validating its low dependency. Different modulation strategies were studied and it was found that SVM presents the best performance for the drive application under the proposed controller.

REFERENCES

[1] C. A. Martins and A. S. Carvalho, "Technological trends in induction motor electrical drives," in *Proc. 2001 IEEE Porto Power Tech Proc.*, 2001, vol. 2, 7 p.

[2] P. Vas and M. Alakula, "Field-oriented control of saturated induction machines," *IEEE Trans. Energy Convers.*, vol. 5, no. 1, pp. 218–224, Mar. 1990.

[3] W. L. Chan, A. T. P. So, and L. L. Lai, "Evolutionary programming based machine parameters estimation for field oriented control," in *Proc. Int. Conf. Electr. Mach. Drives*, 1999, pp. 534–536.

[4] J.-H. Kim, J.-W. Choi, and S.-K. Sul, "Novel rotor flux observer using observer characteristic function in complex vector space for field oriented induction motor drives," in *Proc. 16th Annu. IEEE Appl. Power Electron. Conf. Expo.*, 2001, vol. 1, pp. 615–621.

[5] M. Depenbrock, "Direct self-control (DSC) of inverter-fed induction machine," *IEEE Trans. Power Electron.*, vol. 3, no. 4, pp. 420–429, Oct. 1988.

[6] I. Takahashi and T. Noguchi, "A new quick-response and high-efficiency control strategy of an induction motor," *IEEE Trans. Ind. Appl.*, vol. IA-22, no. 5, pp. 820–827, Sep. 1986.

[7] T. Noguchi, M. Yamamoto, S. Kondo, and I. Takahashi, "High frequency switching operation of PWM inverter for direct torque control of induction motor," in *Proc. Conf. Rec. 1997 IEEE Ind. Appl. Conf. 32nd IAS Annu. Meeting*, 1997, vol. 1, pp. 775–780.

[8] M. P. Kazmierkowski and A. B. Kasprowicz, "Improved direct torque and flux vector control of PWM inverter-fed induction motor drives," *IEEE Trans. Ind. Electron.*, vol. 42, no. 4, pp. 344–350, Aug. 1995.

[9] J. Beerten, J. Verveckken, and J. Driesen, "Predictive direct torque control for flux and torque ripple reduction," *IEEE Trans. Ind. Electron.*, vol. 57, no. 1, pp. 404–412, Jan. 2010.

[10] F. Wang, S. Li, X. Mei, W. Xie, J. Rodriguez, and R. M. Kennel, "Model-based predictive direct control strategies for electrical drives: An experimental evaluation of PTC and PCC methods," *IEEE Trans. Ind. Inf.*, vol. 11, no. 3, pp. 671–681, Jun. 2015.

[11] J. Rengifo, J. Aller, A. Berzoy, and J. Restrepo, "Predictive DTC algorithm for induction machines using Sliding Horizon Prediction," in *Proc. 2014 IEEE 5th Latin Am. Symp. Circuits Syst.*, 2014, pp. 1–4.

[12] L. Djaghdali, S. Belkacem, and F. Naceri, "Reducing of torque and flux ripples in DTC of IM based on predictive control," *J. Electr. Eng.*, vol. 16, pp. 247–257, 2016.

[13] D. Casadei, F. Profumo, G. Serra, and A. Tani, "FOC and DTC: two viable schemes for induction motors torque control," *IEEE Trans. Power Electron.*, vol. 17, no. 5, pp. 779–787, Sep. 2002.

[14] R. Abdelli, D. Rekioua, and T. Rekioua, "Performances improvements and torque ripple minimization for VSI fed induction machine with direct control torque," *ISA Trans.*, vol. 50, no. 2, pp. 213–219, Apr. 2011.

[15] J. C. Viola, J. A. Restrepo, V. M. Guzman, and M. I. Gimenez, "Direct torque control of induction motors using a fuzzy inference system for reduced ripple torque and current limitation," in *Proc. 12th Int. Power Electron. Motion Control Conf.*, 2006, pp. 1161–1166.

[16] G. Noriega, J. Restrepo, A. Bueno, J. M. Aller, M. I. Giménez, and V. Guzmán, "Classic, fuzzy and predictive dtc strategies for the PMSM using the bacterial foraging algorithmas an online parameter estimator," *Rev. Fac. Ing. Univ. Antioquia*, vol. 64, pp. 182–194, Sep. 2012.

[17] Q. Lu, Y. Sun, and S. Mei, *Nonlinear Control Systems and Power System Dynamics*. New York, NY, USA: Springer, 2001.

[18] R. Ortega, N. Barabanov, G. Escobar, and E. Valderrama, "Direct torque control of induction motors: Stability analysis and performance improvement," *IEEE Trans. Autom. Control*, vol. 46, no. 8, pp. 1209–1222, Aug. 2001.

[19] J. Restrepo, J. M. Aller, A. Bueno, V. Guzman, and M. I. Gimenez, "Generalized algorithm for pulse width modulation using a two-vectors based technique," *EPE J.*, vol. 21, no. 2, pp. 30–39, Jun. 2011.

[20] J. Prieto, M. Jones, F. Barrero, E. Levi, and S. Toral, "Comparative analysis of discontinuous and continuous PWM techniques in VSI-fed five-phase induction motor," *IEEE Trans. Ind. Electron.*, vol. 58, no. 12, pp. 5324–5335, Dec. 2011.

[21] L. Asiminoaei, P. Rodriguez, and F. Blaabjerg, "Application of discontinuous PWMModulation in active power filters," *IEEE Trans. Power Electron.*, vol. 23, no. 4, pp. 1692–1706, Jul. 2008.

[22] J. W. R. Santana, J. B. Suñe, J. M. A. Castro, A. A. B. Montilla, and J. A. R. Zambrano, "Parameter estimation method for induction machines using instantaneous voltage and current measurements," *Rev. Fac. Ing.*, no. 75, pp. 57–66, May 2015.

[23] J. Rengifo, J. M. Aller, A. Bueno, J. Viola, and J. Restrepo, "Parameter estimation method for induction machines using the instantaneous impedance during a dynamic start-up," in *Proc. 2012 VI Andean Region Int. Conf.*, 2012, pp. 11–14.

Alberto Berzoy (S'13) received the B.Sc. and M.Sc. degrees in electronics engineering from the Universidad Simon Bolivar, Caracas, Venezuela, in 2003 and 2008, respectively. He is currently working toward the Ph.D. degree in electrical engineering at Florida International University (FIU), Miami, FL, USA, where he has joined the Energy System Research Laboratory.

He is a Teaching Assistant of the Department of Electrical and Computer Engineering, FIU. His research interests include electrical machines, power electronics control and design, electric vehicles, and renewables energies.

Johnny Rengifo received the B.Sc. and M.Sc. degrees in electrical engineering from the Universidad Simón Bolívar (USB), Caracas, Venezuela, in 2008 and 2013, respectively. He is currently working toward the Ph.D. degree in electrical engineering at the Universidad Central de Venezuela, Caracas, Venezuela.

He is currently a Full Professor in the Department of Energy Conversion and Power Delivery, USB. His research interests include electric machines, power electronics, drives, renewable energies, and industrial power systems.

Dr. Osama Mohammed (S'79–M'83–SM'84–F'94) received the M.S. and Ph.D. degrees in electrical engineering from the Virginia Polytechnic Institute and State University, Blacksburg, VA, USA.

He is currently a Full Professor in the Department of Electrical and Computer Engineering, Florida International University, Miami, FL, USA. He has many years of teaching, curriculum development, and research and industrial consulting experience. He authored and coauthored more than 300 technical papers in the archival literature. He specializes in electrical energy systems, in areas related to alternate and renewable energy systems. He is interested in design optimization of electromagnetic devices, artificial intelligence applications as well as electromagnetic field computations. He has a current active and funded research programs by the office of Naval Research and the U.S. Department of Energy.